Retention of activity and secondary structure of hyperthermophilic laccase adsorbed on carbon black

Journal of Physics: Energy

PAPER

Retention of activity and secondary structure of hyperthermophilic laccase adsorbed on carbon black

Takanori Tamaki*, Tomoharu Sugiyama, Yuhei Oshiba and Takeo Yamaguchi

Laboratory for Chemistry and Life Science, Institute of Innovative Research, Tokyo Institute of Technology, Yokohama, Japan

* Author to whom any correspondence should be addressed.

E-mail: tamaki.t.aa@m.titech.ac.jp

Keywords: hyperthermophilic enzyme, mesophilic enzyme, adsorption, deactivation, carbon black, secondary structures

OPEN ACCESS

RECEIVED
28 September 2020

REVISED
31 December 2020

ACCEPTED FOR PUBLICATION
3 February 2021

PUBLISHED
19 March 2021

Abstract

Further increases in the current density of biofuel cells are partly limited by the deactivation of enzymes upon adsorption on hydrophobic carbon materials. A hyperthermophilic enzyme, hyperthermophilic laccase, was employed in the present study and the change in the activities and secondary structures upon adsorption on carbon black (CB) were evaluated by the oxidation rate of 2,2′-azinobis(3-ethylbenzothiazoline-6-sulfonate) and by Fourier transform infrared spectroscopy, respectively, in comparison with the mesophilic enzymes, laccase from *Trametes versicolor* (denoted as mesophilic laccase), and glucose oxidase (GOx). Hyperthermophilic laccase retained its specific activities and secondary structures upon adsorption on CB compared with the other two enzymes mesophilic laccase and GOx.

1. Introduction

The ability of enzymes to oxidize various substances is utilized in biofuel cells to convert the chemical energy of nontoxic fuels to electrochemical energy. Moderate operating conditions for biofuel cells enable their applications in various devices such as wearable [1, 2] and implantable devices [3, 4]. Considering the high intrinsic activity of enzymes, enzymatic biofuel cells have the potential to achieve high power densities that can power portable devices [5–7] and become a key tool for future smart life and smart community. The use of high-surface-area carbon materials, such as carbon nanotubes, carbon black (CB), monolithic carbonaceous foams, and magnesium oxide-templated mesoporous carbon, with rational electrode design has led to an increase in the current density of glucose biofuel cells [6–21]. Our approach is to fabricate a high-surface-area, three-dimensional biofuel cell electrode using redox-polymer-grafted CB. The effectiveness of the approach was demonstrated by applying the electrode to a glucose-oxidizing anode with glucose oxidase (GOx) [8, 9, 12] and an oxygen-reducing cathode with laccase [11], and by developing a mathematical model that considered the reaction and diffusion processes in the electrode [5]. Further investigation of the electrode revealed that deactivation of GOx due to the physical adsorption on the hydrophobic carbon surface limited the utilization ratio of the electrode surface to only a few percent [5, 10]. Thus, deactivation of enzymes upon adsorption on CB is one of the factors preventing high current densities above 10^2 mA cm^{-2}. To solve this problem, one approach is to reduce the physical adsorption and resultant deactivation of enzymes by surface modification of CB [12]. Another approach is to utilize rigid enzymes that can retain their activity and structure upon adsorption on CB.

One important class of very stable proteins are thermophilic proteins that retain their structure and activity at high temperatures [22]. Thermophilic and hyperthermophilic enzymes have been employed as biocatalysts in electrode reactions to increase the operational temperature of biofuel cells. For example, hyperthermophilic [NiFe]-hydrogenase [23–27] and thermophilic pyrroloquinoline quinone dependent glucose dehydrogenase [28] have been employed in the anode reaction, and thermophilic bilirubin oxidase [26, 27, 29–32] and thermophilic laccase [33–35] have been employed in the cathode reaction. A few of these have been used in both the anode and the cathode to construct biofuel cells by using only thermophilic enzymes [26–28]. The thermophilic enzymes are more rigid than their mesophilic counterparts due to a

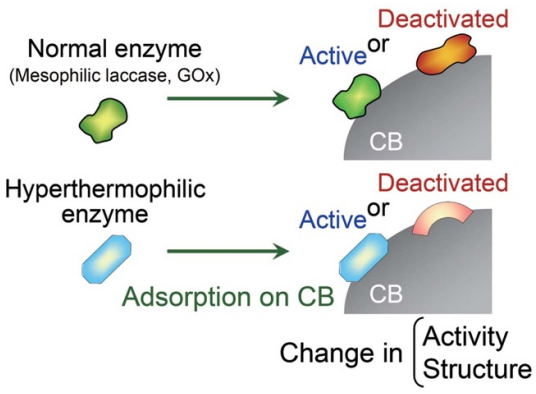

Figure 1. Schematic image of the present study.

variety of structural differences such as more salt bridges, more hydrophobic interactions, and shorter protruding loops [22]. This rigidity can be advantageous for retaining the activity and structure of enzymes upon adsorption on CB.

In the present study, hyperthermophilic laccase with an optimum temperature of approximately 95 °C was employed, and its change in the activities before and after adsorption on CB was compared with that of mesophilic laccase and GOx as shown schematically in figure 1. In addition to the activities, the change in secondary structures upon adsorption on CB was examined by Fourier transform infrared (FT-IR) spectroscopy. Among the characteristic IR absorption bands of proteins, an amide I band around 1700–1600 cm^{-1} is known to be the most sensitive spectral region to the protein secondary structural component [36–39]. In previous studies, the peaks corresponding to amide I band before and after immobilization of laccase or GOx on solid materials were compared to examine the preservation of secondary structures of the enzymes [40–42]. The present study examined the relationship between the change in the activities and the secondary structure of three enzymes, hyperthermophilic laccase, mesophilic laccase, and GOx, upon adsorption on CB.

2. Methods

2.1. Materials

Hyperthermophilic laccase, Laccase YK1, was obtained from Thermostable Enzyme Laboratory Co., Ltd (Kobe, Japan). Mesophilic laccase from *Trametes versicolor* was purchased from Sigma-Aldrich Co. (St. Louis, MO, USA) and purified by ion-exchange chromatography with an NaCl gradient using HiTrap DEAE FF (GE Healthcare, USA). GOx from *Aspergillus niger* was supplied by TOYOBO Co., Ltd (Osaka, Japan). The CB used was Ketjen black with a particle diameter of approximately 30 nm (Lion Corp., Tokyo, Japan). The 2,2′-azinobis(3-ethylbenzothiazoline-6-sulfonate) (ABTS) was purchased from Tokyo Chemical Industry Co., Ltd (Tokyo, Japan). Proteostain Protein Quantification Kit-Rapid, containing Coomassie brilliant blue, was purchased from Dojindo Laboratories (Kumamoto, Japan). The D-gluconic acid/D-gluconolactone assay kit (F-kit) was purchased from JK International Inc. (Tokyo, Japan). All other reagents were purchased from Wako Pure Chemical Industries Ltd (Osaka, Japan) and used without further purification.

2.2. Adsorption of enzymes on CB

Hyperthermophilic laccase and mesophilic laccase was adsorbed on CB as follows. A mixture of 1.0 mg of CB and a buffer solution was stirred for 30 min. The buffer solutions used were 20 mM Tris-HCl buffer solution at pH 8.0 for hyperthermophilic laccase, and 0.1 M acetate buffer solution at pH 4.0 for mesophilic laccase throughout the adsorption of enzymes on CB. Then, hyperthermophilic or mesophilic laccase in the buffer solution was added, and the mixture was stirred for 10 min. The total volume of the solution was 2 ml, and the concentration of laccase was 0.22 mg ml^{-1}. The resulting CB was filtered and washed with the buffer solution. The concentration of hyperthermophilic laccase in the filtrate was determined by absorbance at 280 nm using a calibration curve. The spectra were measured with a U-3310 UV–vis spectrophotometer (Hitachi). The concentration of mesophilic laccase in the filtrate was determined by the Bradford method using Proteostain. The amount of the adsorbed laccase was then obtained by subtracting the amount of laccase in each filtrate from the initial amount of laccase mixed with the CB. The adsorption of GOx on CB and the evaluation of the amount of adsorbed GOx were performed as reported previously [12]; the amount of CB, and the concentration of GOx in the mixture of CB and GOx were 5.0 mg and 0.5 mg ml^{-1}, respectively.

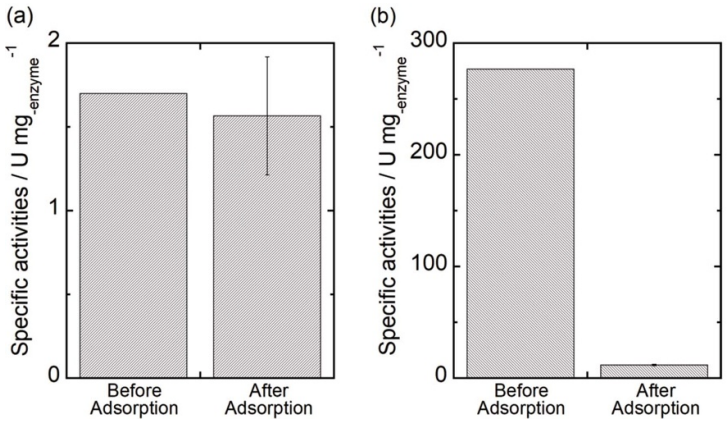

Figure 2. Specific activities of (a) hyperthermophilic and (b) mesophilic laccase before and after adsorption on CB. The data of after adsorption have error bars that denote the standard deviation (SD) of three or more independent experiments.

2.3. Evaluation of the adsorbed enzymes

The activities of adsorbed laccase was determined from the oxidation rate of ABTS. The filtered CB samples with adsorbed laccase were redispersed in the same buffer solution as described in the previous section, and the appropriate volume of each dispersion was added to the mixture of 1 mM ABTS and 1 mM $CuSO_4$ in 0.1 M acetate buffer solution at pH 4.0. The change in absorbance at 405 nm was used for determining the oxidation rate of ABTS. The measurement was performed at 60 °C for hyperthermophilic laccase and at 25 °C for mesophilic laccase. The activities before adsorption on the CB were measured using as-received and purified enzyme solutions for hyperthermophilic and mesophilic laccase, respectively. The activities of adsorbed GOx was determined from the rate of gluconic acid formation using an F-kit as previously reported [12].

The secondary structure of the enzymes before and after adsorption was evaluated using FT-IR spectroscopy. The samples of hyperthermophilic and mesophilic laccase before adsorption on CB were prepared by freeze-drying a solution containing each enzyme. As-received sample was used for the measurement of GOx before adsorption on the CB. Adsorption of enzymes on CB was performed as described in the previous section except that reverse osmosis water was used instead of the buffer solutions. FT-IR spectra were measured with an FT-IR-6200 spectrophotometer (JASCO Co., Ltd) using the KBr pellet technique. Deconvolution of the peak corresponding to the amide I band (1700–1600 cm^{-1}) was performed for the analysis of the secondary structure according to the literature [36–39]. Second derivative of the original spectra was used to identify the number of components and their peak frequencies [36–39]. The Gaussian function was used to fit the spectra [36], and half width at half maximum was set between 7 and 15 cm^{-1} [39]. Curve fitting was performed using Fityk [43] by the Levenberg–Marquardt method using the MINPACK-1 Least Squares Fitting Library in C (MPFIT library). A two-tailed unpaired Student's *t*-test was used to determine statistical significance of proportions of the peak areas before and after adsorption on CB.

3. Results and discussion

3.1. Activities of enzymes adsorbed on CB

The amounts of the adsorbed enzymes on the CB were 0.21 ± 0.03 and 0.11 ± 0.03 mg $mg_{\text{-CB}}^{-1}$ for the hyperthermophilic and mesophilic laccase, respectively. The ratio of the amount of the adsorbed enzymes to the initial amount of the enzymes in the mixture was approximately 20%–50%.

The activities of adsorbed laccase was measured by dispersing a laccase-adsorbed CB sample in ABTS solution. Figure 2 shows the specific activities of hyperthermophilic and mesophilic laccase before and after adsorption on CB, calculated by dividing the activities by the amount of enzymes.

Hyperthermophilic laccase retained its specific activities upon adsorption on CB, while the adsorbed mesophilic laccase greatly decreased its specific activities. It should be noted, however, that the initial specific activities of mesophilic laccase was much higher than that of hyperthermophilic laccase, and thus the specific activities of adsorbed mesophilic laccase, although greatly decreased from its initial value, was still higher than that of adsorbed thermophilic laccase. Figure 3 summarizes the relative activities of hyperthermophilic and mesophilic laccase, defined as the specific activities after adsorption on CB divided by that before adsorption. The relative activity of hyperthermophilic laccase was 92 ± 21%, while that of mesophilic laccase was 4 ± 2%. The decrease in the specific activities upon adsorption on unmodified CB was also observed for

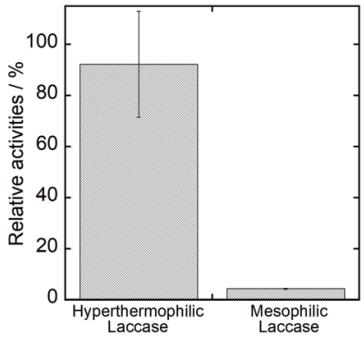

Figure 3. Relative activities of hyperthermophilic laccase and mesophilic laccase upon adsorption on CB. All the data have error bars that denote SD of three independent experiments.

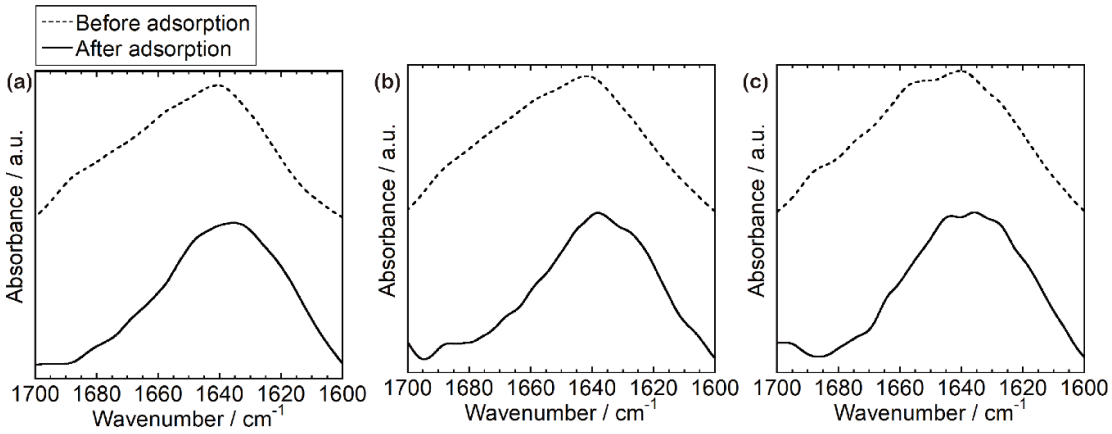

Figure 4. FT-IR spectra of (a) hyperthermophilic laccase, (b) mesophilic laccase, and (c) GOx before and after adsorption on CB. Dotted and solid lines represent IR spectra before and after adsorption, respectively.

mesophilic GOx [10, 12] with the relative activity of 12 ± 3%, when adsorption was performed as reported previously [12].

Electrochemical activities of the enzymes were then evaluated over time by immobilizing the enzymes on CB electrodes. However, the enzymes were detached from the electrodes' surfaces, and thus, the intrinsic durability of the enzymes was not properly evaluated. For the electrochemical application of hyperthermophilic laccase, an efficient immobilization method is necessary to fully utilize the intrinsic durability of the enzyme with other factors such as the proper immobilization of mediators and/or enzyme orientation at an electrode surface and substrate accessibility. Electrochemical application of hyperthermophilic enzymes regarding the abovementioned factors is a topic of future studies.

Further, to investigate the reason for the retention of the specific activities of hyperthermophilic laccase, the change in secondary structures was examined.

3.2. Change in secondary structures of enzymes upon adsorption on CB

The FT–IR spectra of the peak corresponding to the amide I band of the three enzymes before and after adsorption on CB are shown in figure 4. A change in the peak was observed upon adsorption on CB. Deconvolution of the peak was performed to further examine the change in secondary structure. In order to guarantee the uniqueness of the deconvolution, a minimum number of components was used to fit the spectra [36, 39], and the number of components and their peak frequencies after the adsorption on CB were assumed to be the same as those before the adsorption. Figure 5 shows the second derivative of the spectra of the enzymes before the adsorption on the CB. The number of components was identified to be six for the three enzymes with the peak frequencies of 1688, 1675, 1658, 1639, 1628, and 1606 cm^{-1} for hyperthermophilic laccase; 1689, 1674, 1658, 1640, 1627, and 1606 cm^{-1} for mesophilic laccase; and 1688, 1674, 1658, 1639, 1627, and 1607 cm^{-1} for GOx. The deconvolved spectra are shown in figure 6. The components were assigned to the secondary structures according to previous studies [36–42, 44–48], and the results of the deconvolution are summarized in table 1. The proportion of the peak areas for the three enzymes changed to some extent upon the adsorption on CB. Among the secondary structures, changes in

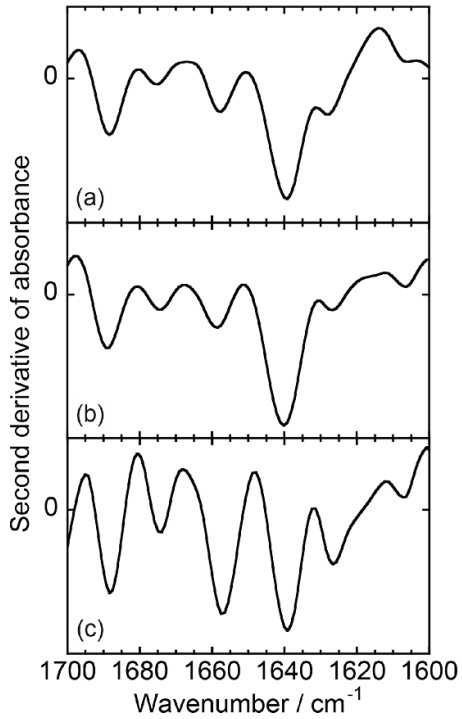

Figure 5. Second derivative of the spectra of (a) hyperthermophilic laccase, (b) mesophilic laccase, and (c) GOx before adsorption on CB.

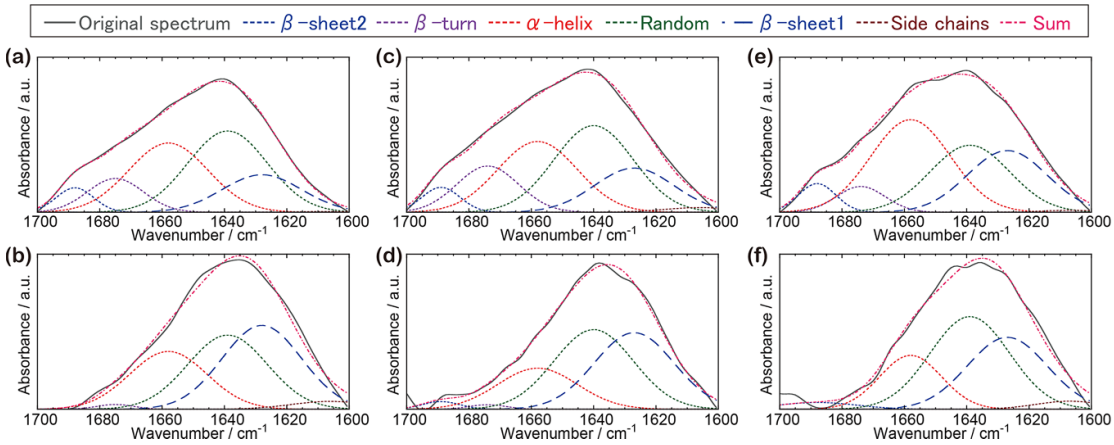

Figure 6. Deconvolved amide I band of (a), (b) hyperthermophilic laccase, (c), (d) mesophilic laccase, and (e), (f) GOx before (a), (c), (e) and after (b), (d), (f) adsorption on CB.

Table 1. Secondary structures of hyperthermophilic laccase, mesophilic laccase, and GOx before and after adsorption on CB: assignments of components and proportion of peak area. Mean ± SD of at least three independent experiments is shown.

Peak frequencies (cm^{-1})		1689/1688, 1628/1627	1675/1674	1658	1640/1639	1607/1606
Assignment		β-sheet	β-turn	α-helix	Random	Side chain
Proportion of peak area		%	%	%	%	%
Hyperthermophilic laccase	Before adsorption	23 ± 3	10 ± 1	31 ± 1	36 ± 0	0 ± 0
	After adsorption	30 ± 8	1 ± 0	23 ± 3	40 ± 8	6 ± 3
Mesophilic laccase	Before adsorption	23 ± 2	12 ± 2	30 ± 1	33 ± 1	2 ± 0
	After adsorption	37 ± 8	0 ± 1	13 ± 9	46 ± 6	4 ± 4
GOx	Before adsorption	34 ± 8	5 ± 1	39 ± 3	19 ± 10	3 ± 4
	After adsorption	33 ± 8	1 ± 1	18 ± 5	44 ± 8	4 ± 2

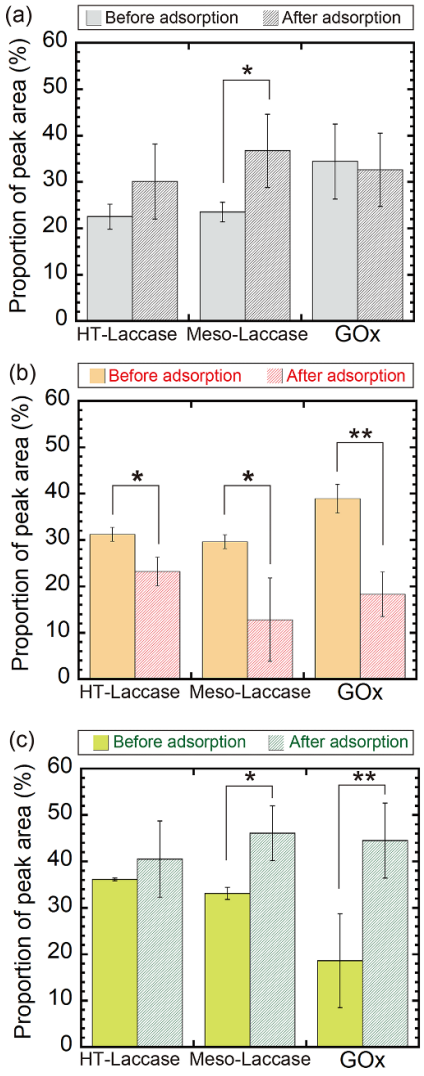

Figure 7. Proportion of the peak areas of the (a) β-sheet, (b) α-helix, and (c) random portions of hyperthermophilic laccase (HT-Laccase), mesophilic laccase (Meso-Laccase), and GOx before and after adsorption on CB; the error bars denote the SD of at least three independent experiments; and the asterisks denote a significant difference before and after adsorption on CB: * $p < 0.05$, ** $p < 0.01$.

proportion of β-sheet, α-helix, and random portions have been discussed in relation to the activities of enzymes [44, 48, 49]. Figure 7 shows the proportions of the peak areas of β-turn, α-helix, and random portions before and after the adsorption on the CB. A decrease in the α-helix upon the adsorption on the CB was observed for all three enzymes. Concomitantly, the β-sheet and random portions increased for the mesophilic laccase, and random portions increased for the glucose oxidase upon the adsorption on the CB. On the other hand, the changes in the proportions of the β-sheet and random portions of the hyperthermophilic laccase were not statistically significant. Thus, compared with the mesophilic laccase and glucose oxidase, the hyperthermophilic laccase retained its entire structure. The crystal structure of Laccase from *Trametes versicolor* (denoted as mesophilic laccase in this article) shows that α-helix and 3_{10}-helix, whose peak frequencies are similar to α-helix [38], play important roles such as carrying the type-1 copper ligating histidine and connecting regions between the domains [50]. As for GOx, α-helix is a part of the flavin adenine dinucleotide (FAD) binding domain, and is in the focal point of the bent six-stranded antiparallel β-sheet of the substrate binding domain [51]. Thus, decrease in the proportion of an α-helix can greatly affect the structure and activity of mesophilic laccase and GOx. Actually, the thermal denaturation of GOx results in the loss of α-helix and increase in the unordered structure [46]. From the abovementioned discussion, the decrease in the specific activities of the mesophilic laccase and GOx could be attributed to the decrease in the proportion of the α-helix and concomitant increase in the other components upon the adsorption on the CB. On the other hand, the relatively small change in the entire structure was observed for the hyperthermophilic laccase compared with the other two enzymes. This smaller change is possibly due to the rigid structure of the enzyme. To further understand the reasons for the high retention of the specific

activity and secondary structures of the hyperthermophilic laccase, which is possibly owing to its rigid structure, the comparison of its sequence with other enzymes and modeling of its secondary, tertiary, and quaternary structures are required. Clarification of the structure of the enzyme will be a topic of future studies.

4. Conclusion

Further increase in the current density of biofuel cells requires a decrease in the deactivation of enzymes upon adsorption on hydrophobic carbon materials that function as a high-surface-area three-dimensional electrode. Comparison of the activities and the FT-IR spectra of hyperthermophilic laccase, mesophilic laccase, and GOx before and after adsorption on CB revealed that hyperthermophilic laccase retained its specific activities and secondary structures upon adsorption on CB compared with the other two enzymes, mesophilic laccase and GOx. Preservation of the specific activities and secondary structures may be attributed to the rigid structure of hyperthermophilic laccase, which implies that rigid enzymes could be candidates for enzymes that are not deactivated upon adsorption on hydrophobic carbon materials.

Acknowledgments

The authors would like to thank Thermostable Enzyme Laboratory Co., Ltd for supplying hyperthermophilic laccase, and TOYOBO Co., Ltd for supplying GOx. This work was supported by JSPS KAKENHI Grant No. JP18K04822, and was also supported in part by ”Five-star Alliance”.

ORCID iDs

Takanori Tamaki https://orcid.org/0000-0002-7728-9397
Yuhei Oshiba https://orcid.org/0000-0002-6029-3293
Takeo Yamaguchi https://orcid.org/0000-0001-9043-4408

References

[1] Kim J, Campbell A S, De Avila B E F and Wang J 2019 Wearable biosensors for healthcare monitoring *Nat. Biotechnol.* **37** 389–406
[2] Shitanda I, Fujimura Y, Nohara S, Hoshi Y, Itagaki M and Tsujimura S 2019 Paper-based disk-type self-powered glucose biosensor based on screen-printed biofuel cell array *J. Electrochem. Soc.* **166** B1063–8
[3] Gross A J, Holzinger M and Cosnier S 2018 Buckypaper bioelectrodes: emerging materials for implantable and wearable biofuel cells *Energy Environ. Sci.* **11** 1670–87
[4] Shleev S 2017 Quo vadis, implanted fuel cell? *Chempluschem* **82** 522–39
[5] Tamaki T, Ito T and Yamaguchi T 2009 Modelling of reaction and diffusion processes in a high-surface-area biofuel cell electrode made of redox polymer-grafted carbon *Fuel Cells* **9** 37–43
[6] Tamaki T 2012 Enzymatic biofuel cells based on three-dimensional conducting electrode matrices *Top. Catal.* **55** 1162–80
[7] Tamaki T 2017 *Biocatalysis and Nanotechnology* ed P Grunwald (Singapore: Pan Stanford Publishing Pte. Ltd) p 595
[8] Tamaki T and Yamaguchi T 2006 High-surface-area three-dimensional biofuel cell electrode using redox-polymer-grafted carbon *Ind. Eng. Chem. Res.* **45** 3050–8
[9] Tamaki T, Ito T and Yamaguchi T 2007 Immobilization of hydroquinone through a spacer to polymer grafted on carbon black for a high-surface-area biofuel cell electrode *J. Phys. Chem.* B **111** 10312–9
[10] Tamaki T, Hiraide A, Asmat F B, Ohashi H, Ito T and Yamaguchi T 2010 Evaluation of immobilized enzyme in a high-surface-area biofuel cell electrode made of redox-polymer-grafted carbon black *Ind. Eng. Chem. Res.* **49** 6394–8
[11] Sugiyama T, Tamaki T and Yamaguchi T 2014 Development of redox polymer grafted onto carbon black using 2,2′-azinobis(3-ethylbenzothiazoline-6-sulfonic acid) as a biocathode *J. Chem. Eng. Japan* **47** 704–10
[12] Tamaki T, Sugiyama T, Mizoe M, Oshiba Y and Yamaguchi T 2014 Reducing physical adsorption of enzymes by surface modification of carbon black for high-current-density biofuel cells *J. Electrochem. Soc.* **161** H3095–9
[13] Sakai H, Nakagawa T, Tokita Y, Hatazawa T, Ikeda T, Tsujimura S and Kano K 2009 A high-power glucose/oxygen biofuel cell operating under quiescent conditions *Energy Environ. Sci.* **2** 133–8
[14] Hickey D P, Halmes A J, Schmidtke D W and Glatzhofer D T 2014 Electrochemical characterization of glucose bioanodes based on tetramethylferrocene-modified linear poly(ethylenimine) *Electrochim. Acta* **149** 252–7
[15] Barton S C, Sun Y H, Chandra B, White S and Hone J 2007 Mediated enzyme electrodes with combined micro- and nanoscale supports *Electrochem. Solid State Lett.* **10** B96–100
[16] Yoshino S, Miyake T, Yamada T, Hata K and Nishizawa M 2013 Molecularly ordered bioelectrocatalytic composite inside a film of aligned carbon nanotubes *Adv. Energy Mater.* **3** 60–4
[17] Flexer V, Brun N, Backov R and Mano N 2010 Designing highly efficient enzyme-based carbonaceous foams electrodes for biofuel cells *Energy Environ. Sci.* **3** 1302–6
[18] Flexer V, Brun N, Destribats M, Backov R and Mano N 2013 A novel three-dimensional macrocellular carbonaceous biofuel cell *Phys. Chem. Chem. Phys.* **15** 6437–45
[19] Tsujimura S, Murata K and Akatsuka W 2014 Exceptionally high glucose current on a hierarchically structured porous carbon electrode with ‘wired’ flavin adenine dinucleotide-dependent glucose dehydrogenase *J. Am. Chem. Soc.* **136** 14432–7
[20] Suzuki A, Mano N and Tsujimura S 2017 Lowering the potential of electroenzymatic glucose oxidation on redox hydrogel-modified porous carbon electrode *Electrochim. Acta* **232** 581–5

[21] Niiyama A, Murata K, Shigemori Y, Zebda A and Tsujimura S 2019 High-performance enzymatic biofuel cell based on flexible carbon cloth modified with MgO-templated porous carbon *J. Power Sources* **427** 49–55
[22] Petsko G A and Ringe D 2004 *Protein Structure and Function* (London: New Science Press Ltd)
[23] Luo X J, Brugna M, Tron-Infossi P, Giudici-Orticoni M T and Lojou E 2009 Immobilization of the hyperthermophilic hydrogenase from *Aquifex aeolicus* bacterium onto gold and carbon nanotube electrodes for efficient H_2 oxidation *J. Biol. Inorg. Chem.* **14** 1275–88
[24] Ciaccafava A, De Poulpiquet A, Techer V, Giudici-Orticoni M T, Tingry S, Innocent C and Lojou E 2012 An innovative powerful and mediatorless H_2/O_2 biofuel cell based on an outstanding bioanode *Electrochem. Commun.* **23** 25–8
[25] De Poulpiquet A, Ciaccafava A, Szot K, Pillain B, Infossi P, Guiral M, Opallo M, Giudici-Orticoni M T and Lojou E 2013 Exploring properties of a hyperthermophilic membrane-bound hydrogenase at carbon nanotube modified electrodes for a powerful H_2/O_2 biofuel cell *Electroanalysis* **25** 685–95
[26] De Poulpiquet A, Ciaccafava A, Gadiou R, Gounel S, Giudici-Orticoni M T, Mano N and Lojou E 2014 Design of a H_2/O_2 biofuel cell based on thermostable enzymes *Electrochem. Commun.* **42** 72–4
[27] Mazurenko I, Monsalve K, Infossi P, Giudici-Orticoni M T, Topin F, Mano N and Lojou E 2017 Impact of substrate diffusion and enzyme distribution in 3D-porous electrodes: a combined electrochemical and modelling study of a thermostable H_2/O_2 enzymatic fuel cell *Energy Environ. Sci.* **10** 1966–82
[28] Wang X Y, Li D, Watanabe T, Shigemori Y, Mikawa T, Okajima T, Mao L Q and Ohsaka T 2012 A glucose/O_2 biofuel cell using recombinant thermophilic enzymes *Int. J. Electrochem. Sci.* **7** 1071–8 (http://www.electrochemsci.org/papers/vol7/7021071.pdf)
[29] Suraniti E, Tsujimura S, Durand F and Mano N 2013 Thermophilic biocathode with bilirubin oxidase from Bacillus pumilus *Electrochem. Commun.* **26** 41–4
[30] Tsujimura S, Suraniti E, Durand F and Mano N 2014 Oxygen reduction reactions of the thermostable bilirubin oxidase from Bacillus pumilus on mesoporous carbon-cryogel electrodes *Electrochim. Acta* **117** 263–7
[31] Mazurenko I *et al* 2016 How the intricate interactions between carbon nanotubes and two bilirubin oxidases control direct and mediated O_2 reduction *ACS Appl. Mater. Interfaces* **8** 23074–85
[32] De Poulpiquet A *et al* 2017 Mechanism of chloride inhibition of bilirubin oxidases and its dependence on potential and pH *ACS Catal.* **7** 3916–23
[33] Beneyton T, Beyl Y, Guschin D A, Griffiths A D, Taly V and Schuhmann W 2011 The thermophilic CotA laccase from *Bacillus subtilis*: bioelectrocatalytic evaluation of O_2 reduction in the direct and mediated electron transfer regime *Electroanalysis* **23** 1781–9
[34] Beneyton T, El Harrak A, Griffiths A D, Hellwig P and Taly V 2011 Immobilization of CotA, an extremophilic laccase from *Bacillus subtilis*, on glassy carbon electrodes for biofuel cell applications *Electrochem. Commun.* **13** 24–7
[35] Liu X, Gillespie M, Ozel A D, Dikici E, Daunert S and Bachas L G 2011 Electrochemical properties and temperature dependence of a recombinant laccase from *Thermus thermophilus Anal. Bioanal. Chem.* **399** 361–6
[36] Byler D M and Susi H 1986 Examination of the secondary structure of proteins by deconvolved FTIR spectra *Biopolymers* **25** 469–87
[37] Susi H and Byler D M 1983 Protein-structure by Fourier-transform infrared-spectroscopy—2nd derivative spectra *Biochem. Biophys. Res. Commun.* **115** 391–7
[38] Kong J and Yu S 2007 Fourier transform infrared spectroscopic analysis of protein secondary structures *Acta Biochim. Biophys. Sin.* **39** 549–59
[39] Hiramatsu M 2009 Secondary structure analysis of proteins using infrared adsorption spectroscopy *PSSJ Arch.* **2** e054 (in Japanese)
[40] Ahn M Y, Zimmerman A R, Martinez C E, Archibald D D, Bollag J M and Dec J 2007 Characteristics of *Trametes villosa* laccase adsorbed on aluminum hydroxide *Enzyme Microb. Technol.* **41** 141–8
[41] Delfino I, Portaccio M, Della Ventura B, Mita D G and Lepore M 2013 Enzyme distribution and secondary structure of sol-gel immobilized glucose oxidase by micro-attenuated total reflection FT-IR spectroscopy *Mater. Sci. Eng.* C **33** 304–10
[42] Zhao H Z, Sun J J, Song J and Yang Q Z 2010 Direct electron transfer and conformational change of glucose oxidase on carbon nanotube-based electrodes *Carbon* **48** 1508–14
[43] Wojdyr M 2010 Fityk: a general-purpose peak fitting program *J. Appl. Crystallogr.* **43** 1126–8
[44] Guiomar A J, Guthrie J T and Evans S D 1999 Use of mixed self-assembled monolayers in a study of the effect of the microenvironment on immobilized glucose oxidase *Langmuir* **15** 1198–207
[45] Haouz A, Twist C, Zentz C, Tauc P and Alpert B 1998 Dynamic and structural properties of glucose oxidase enzyme *Eur. Biophys. J. Biophys. Lett.* **27** 19–25
[46] Wang Q A, Xu W, Wu P, Zhang H, Cai C X and Zhao B 2010 New insights into the effects of thermal treatment on the catalytic activity and conformational structure of glucose oxidase studied by electrochemistry, IR spectroscopy, and theoretical calculation *J. Phys. Chem.* B **114** 12754–64
[47] Agrawal K and Verma P 2020 Multicopper oxidase laccases with distinguished spectral properties: a new outlook *Heliyon* **6** e03972
[48] Ragusa S, Cambria M T, Pierfederici F, Scire A, Bertoli E, Tanfani F and Cambria A 2002 Structure-activity relationship on fungal laccase from *Rigidoporus lignosus*: a Fourier-transform infrared spectroscopic study *Biochim. Biophys. Acta Proteins Proteom.* **1601** 155–62
[49] Gouda M D, Singh S A, Rao A G A, Thakur M S and Karanth N G 2003 Thermal inactivation of glucose oxidase—mechanism and stabilization using additives *J. Biol. Chem.* **278** 24324–33
[50] Piontek K, Antorini M and Choinowski T 2002 Crystal structure of a laccase from the fungus *Trametes versicolor* at 1.90 Å resolution containing a full complement of coppers *J. Biol. Chem.* **277** 37663–9
[51] Hecht H J, Kalisz H M, Hendle J, Schmid R D and Schomburg D 1993 Crystal structure of glucose oxidase from *Aspergillus niger* refined at 2.3 Å resolution *J. Mol. Biol.* **229** 153–72